

SDSS J092609.45+334304.1: a nearby unevolved galaxy

S.A. Pustilnik,^{1,5*} A.L. Tepliakova,¹ A.Y. Kniazev,^{2,3} J.-M. Martin,⁴ and A.N. Burenkov¹

¹ *Special Astrophysical Observatory of RAS, Nizhnij Arkhyz, Karachai-Circassia 369167, Russia*

² *South African Astronomical Observatory, PO Box 9, 7935 Observatory, Cape Town, South Africa*

³ *Southern African Large Telescope Foundation, PO Box 9, 7935 Observatory, Cape Town, South Africa*

⁴ *GEPI and Station de radioastronomie, Observatoire de Paris, 5 place Jules Janssen, 92190 Meudon, France*

⁵ *Isaac Newton Institute of Chile, SAO branch, Nizhnij Arkhyz, Russia*

Accepted 2009 August 30. Received 2009 July 3

ABSTRACT

We present the results of observations of the very low surface brightness (VLSB) dwarf galaxy SDSS J092609.45+334304.1 with extreme parameters which indicate its unevolved status. Namely, its value of O/H, derived as an average of that in two adjacent H II regions at the NE edge of the disc, corresponds to the parameter $12+\log(\text{O}/\text{H})=7.12\pm 0.02$, which is amongst two lowest known. The total HI flux measurement obtained with the Nançay Radio Telescope and the photometric results imply that the galaxy ratio $M(\text{HI})/L_B \sim 3.0$, is among the top known in the Local Volume. The galaxy is situated in the region of a nearby underdense region known as the Lynx-Cancer void, where other, unevolved galaxies, including DDO 68, HS 0832+3542 and SAO 0822+3545, are known to be present. The total mass of this almost edge-on VLSB galaxy is ~ 8.3 times larger than its baryonic mass, implying the dynamical dominance of Dark Matter (DM) halo. The $(u - g)$, $(g - r)$ colours of outer parts of this galaxy are consistent with the ages of its main stellar population of 1–3 Gyr. Thanks to the galaxy isolation, the small effect of current or recent star formation (SF), its proximity and rather large HI flux ($\sim 2.5 \text{ Jy}\cdot\text{km s}^{-1}$), this VLSB dwarf is a good laboratory for the detailed study of DM halo properties through HI kinematics and the star formation processes in very metal-poor low surface density environment. This finding, along with the discovery of other unusual dwarf galaxies in this void, provides evidence for the relation between galaxy evolution and its very low-density environment for the baryonic mass range of 10^8 to $10^9 M_\odot$. This relation seems to be consistent with that expected in the Λ CDM models of galaxy and structure formation.

Key words: galaxies: dwarf – galaxies: evolution – galaxies: abundances – galaxies: photometry – galaxies: individual: SDSS J092609.45+334304.1 – cosmology: large-scale structure of Universe

1 INTRODUCTION

The modern cosmological CDM models of the large-scale structure and galaxy formation, including the state-of-art N-body simulations, predict that galaxy properties and evolution can significantly depend on their global environment (e.g., Peebles 2001; Mathis & White 2002; Gottlöber et al. 2003; Hoeft et al. 2006; Arkhipova et al. 2007; Hahn et al. 2007, 2009, and references therein). While the effect of a denser environment on galaxy properties and evolution is known for rather long time (e.g., Haynes, Giovanelli & Chincarini 1984), the role of the most

rarefied environment (typical of voids) on galaxy formation and evolution is less studied both theoretically and observationally. For observational aspects, various selection effects must be taken into account. In particular, most galaxies with known radial velocities come from spectral surveys of magnitude-limited samples. Wide-field spectral surveys have typical magnitude limits corresponding roughly to $B \sim 18$. This apparent magnitude limit implies that for distances well beyond the Local Supercluster ($cz > 5000 - 6000 \text{ km s}^{-1}$), where large voids were found, the faintest selected galaxies will have the absolute magnitudes M_B of ~ -16 or higher. This implies that the study of distant voids is limited by the galaxies with M_B of only $\sim 2-3$ mag. fainter than that corresponding to the luminosity of

* E-mail: sap@sao.ru (SAP)

L_* ($M_B^* \sim -19.5$). The latter (or close to this) is usually used for selection of galaxies delineating the borders of ‘empty’ regions - voids. Therefore, even the most advanced studies of void galaxy population, based on very large samples with redshifts from the Sloan Digital Sky Survey (SDSS) (e.g., Sorrentino, Antonuccio-Delogu & Rifatto 2006; Patiri et al. 2006) of $z < 0.03-0.05$, were limited by the galaxy samples with luminosities only 1.5-2 magnitudes fainter than $M_B^* \sim -19.5$. Since the possible difference of galaxy properties in various types of environment is expected to depend on galaxy mass, these ‘shallow’ probes of ‘distant’ void galaxy population, based on the SDSS samples, may be inadequate to get deeper insights into the questions.

In order to probe the properties of smaller luminosities void galaxies, a wide-angle redshift survey with a similar magnitude limit is needed, for a volume located several times closer than those used in the previous studies. Apart from the giant Local Void described by Tully et al. (2008), which extends to tens Mpc and appears almost empty, several relatively small voids adjacent to the Local Volume (defined by $D < 10$ Mpc, e.g., Karachentsev et al. 2004) are identified (see Fairall 1998). One more such void in Lynx-Cancer sky region was noticed by Pustilnik et al. (2003). Due to its relative proximity ($D_{\text{centre}} \sim 14$ Mpc), galaxies selected in this region for the SDSS spectroscopy, have the absolute magnitudes down to M_B of $-(12.5-13.0)$. Studying the dwarf galaxies population in nearby voids, and in particular, in this Lynx-Cancer void, will permit to advance significantly in probing void dwarf galaxy properties. This will also give a base for a comparison of the *evolutionary status* of void dwarf galaxies and those located in the regions with the higher galaxy density.

Coming back to the study of void galaxy population, it is worth noting the well known correlation between galaxy luminosities and their central surface brightnesses (e.g., Cross & Driver 2002, and references therein). Since most of voids galaxies are dwarfs (as seen, in particular, in the sample of galaxies falling on Lynx-Cancer void), with the major fraction by number of low luminosities, the proportion of LSB galaxies in voids is expected to be also higher. In the SDSS project, relatively high surface brightness (SB) lower limits have been used for spectroscopic target selection. Therefore, the completeness for the SDSS redshift samples falls below 50% for objects with the half-light $\mu_{50,r} \geq 23.5$ mag arcsec $^{-2}$ (e.g., Geha et al. 2006). Hence, the resulting SDSS galaxy samples with redshifts are biased against LSB galaxies and this can lead to a substantial loss of LSB dwarf galaxies in void galaxy samples. Some of these missing galaxies might form the youngest local galaxy population (Zackrisson, Bergvall & Östlin 2005).

Blind HI surveys can overcome this selection effect, at least for late-type galaxies. Therefore, one can expect that the Arecibo blind HI survey ALFALFA (e.g., Haynes 2008) will further increase the current Lynx-Cancer void dwarf sample and will find mainly LSBD new galaxies. The currently available dwarf sample includes about fifty late-type galaxies (Pustilnik et al., in preparation).

During the systematic study of dwarf galaxies in the Lynx-Cancer void we have already discovered several unusual objects, including DDO 68 (Pustilnik, Kniazev & Pramskij 2005; Izotov & Thuan 2007; Pustilnik, Tepliakova & Kniazev 2008a),

HS 0822+3542, SAO 0822+3545 (Kniazev et al. 2000; Pustilnik et al. 2003; Chengalur et al. 2006). In this paper we report on the case study of one of the Lynx-Cancer void genuine LSB dwarfs, which passed through the SDSS spectral target SB selection criterion because of its almost edge-on viewing direction and its brightening in apparent SB. It appeared as an extremely metal-poor and very gas-rich galaxy located remarkably close to DDO 68. The paper is organised as follows. In Section 2 we briefly describe the observations and the reduction of obtained data. Section 3 presents the results of observations and their analysis. In Section 4 we discuss the results and their implications in a broader context and summarise our conclusions.

2 OBSERVATIONS AND DATA REDUCTION

2.1 Optical observations

The long-slit spectral observations of galaxy SDSS J092609.45+334304.1 (hereafter J0926+3343 for brevity, see its main parameters in Table 6) were conducted with the multimode instrument SCORPIO (Afanasiev & Moiseev 2005) installed at the prime focus of the SAO 6 m telescope (BTA) on the nights of 2008 November 26, 2009 January 21 and 22, and 2009 February 19. The grism VPHG550G was used with the 2K×2K CCD detector EEV 42-40 on 2008 November 26 and 2009 February 19. On 2009 January 21 and 22, the grisms VPHG1200G and VPHG550G with the 2K×4K CCD detector EEV 42-90 were used. The respective spectral ranges, spectral resolution, exposure times and seeings are presented in Table 1. The scale along the slit (after binning) was 0''36 pixel $^{-1}$ in all cases. The object spectra were complemented before or after by the reference spectra of He-Ne-Ar lamp for the wavelength calibration. The spectral standard star Feige 34 (Bohlin 1996) was observed during the nights for the flux calibration.

The long slit was positioned on the two H II regions **a** and **b** on the NE edge of SDSS J0926+3343 edge-on disc (see images of the galaxy in the SDSS *g*-filter and BTA filter SED665 in Fig. 1). These H II regions (with a distance of $\sim 4''$ in between) were identified through one-minute exposure acquisition images of this galaxy with the medium-width filter SED665, centred at $\lambda 6622$ Å and with FWHM=191 Å. The slit was centred on these H II regions. Its direction was not along the disc major axis. The spectrum of one more, a fainter H II region **c** at $\sim 17''$ from **b**, close to the galaxy centre, was acquired at this slit orientation. We notice that the region **c** is different from the very faint region, labeled in Fig. 1 as **e**, for which the SDSS spectrum was obtained. The latter is situated at $\sim 31''$ from region **b**.

All spectral data reduction and emission line measurements were performed similar to that described in Pustilnik et al. (2005). Namely, the standard pipeline with the use of IRAF¹ and MIDAS² was applied for the reduc-

¹ IRAF: the Image Reduction and Analysis Facility is distributed by the National Optical Astronomy Observatory, which is operated by the Association of Universities for Research in Astronomy, Inc. (AURA) under cooperative agreement with the National Science Foundation (NSF).

² MIDAS is an acronym for the European Southern Observatory package – Munich Image Data Analysis System.

Table 1. Journal of the 6 m telescope observations of SDSS J0926+3343

Date	Exposure time [s]	Wavelen.Range [Å]	Dispersion [Å/pixel]	Spec.resol. FWHM(Å)	Seeing [arcsec]	Airmass	Grism	Detector
(1)	(2)	(3)	(4)	(5)	(6)	(7)	(8)	(9)
2008.11.26	4×900	3500 – 7500	2.1	12.0	2.3	1.11	VPHG550G	2K×2K
2009.01.21	6×900	3700 – 5700	0.9	5.5	1.3	1.11	VPHG1200G	2K×4K
2009.01.22	4×900	3600 – 9000	2.1	12.0	1.5	1.02	VPHG550G	2K×4K
2009.02.19	8×900	3500 – 7500	2.1	12.0	1.9	1.05	VPHG550G	2K×2K

tion of long-slit spectra, which included the following steps: removal of cosmic ray hits, bias subtraction, flat-field correction, wavelength calibration, night-sky background subtraction. Then, using the data on the spectrophotometry standard star, all spectra were transformed to absolute fluxes. We could extract individual 1D spectra of regions **a** and **b** only for nights 2009.01.21 and 2009.01.22. This was done by summing up without weighting of 6 and 10 rows along the slit, respectively.

In order to derive the estimate of the galaxy O/H using all obtained data, we extracted also for every night the light of the ‘composite’ spectrum, containing both regions **a** and **b**, summing up without weighting 21 rows ($\sim 7.5''$) along the slit (see more details in Section 3). The emission line intensities with their errors were measured in the way described in detail in Kniazev et al. (2004a).

2.2 HI observations

The HI-observations with the Nançay³ radio telescope (NRT) with a collecting area of 200×34.5 m are characterised by a half-power beam width (HPBW) of $3.7'$ (East-West) $\times 22'$ (North-South) at declination $\delta=0^\circ$ (see also <http://www.obs-nancay.fr/nrt>). The data were acquired during July-September 2007, with the total time on-source of ~ 6 hours. We used the antenna/receiver system F.O.R.T. (e.g., Martin et al. 2002) with improved overall sensitivity. The system temperature was ~ 35 K for both the horizontal and vertical linear polarisations of a dual-polarisation receiver. The gain of the telescope was 1.5 K Jy^{-1} at declination $\delta=0^\circ$. The 8192-channel correlator was used covering a total bandwidth of 12.5 MHz. The total velocity range covered was about 2700 km s^{-1} , with the channel spacing of 1.3 km s^{-1} before smoothing. The observations consisted of separate cycles of ‘ON’ and ‘OFF’ integrations, each of 40 seconds in duration. ‘OFF’ integrations were acquired at the target declination, with the East R.A. offset of $\sim 15' \times \cos(\delta)$. For more detail see the description in the paper by Pustilnik & Martin (2007).

The data were reduced using the NRT standard programs NAPS and SIR, written by the telescope staff (see description on <http://www.obs-nancay.fr/nrt/support>). Horizontal and vertical polarisation spectra were calibrated and

processed independently and then averaged together. The error estimates were calculated following Schneider et al. (1986). The baselines were generally well-fit by a third order or lower polynomial and were subtracted out.

2.3 Imaging data from the SDSS

The SDSS (York et al. 2000) is well suited for photometric studies of various galaxy samples due to its homogeneity, area coverage, and depth (SDSS Project Book⁴). SDSS is an imaging and spectroscopic survey that covers about one-quarter of the Celestial Sphere. The imaging data are collected in drift scan mode in five bandpasses (u , g , r , i , and z ; Fukugita et al. 1996) using mosaic CCD camera (Gunn et al. 2003). An automated image-processing system detects astronomical sources and measures their photometric and astrometric properties (Lupton et al. 2001; Smith et al. 2002; Pier et al. 2003) and identifies candidates for multi-fibre spectroscopy. At the same time, the pipeline-reduced SDSS data can be used, if necessary, in order to get independent photometry (e.g., Kniazev et al. 2004b). For our current study the images in the respective filters were retrieved from the SDSS Data Release 7 (DR7; Abazajian et al. 2009).

Since the SDSS provides users with the fully reduced images, the only additional step we needed to perform (apart from the photometry in round diaphragms) was the background subtraction. For this, all bright stars were removed from the images. After that the studied object was masked and the background level within this mask was approximated with the package `aip` from MIDAS. In more detail the method and the related programs are described in Kniazev et al. (2004b). To transform instrumental fluxes in diaphragms to stellar magnitudes, we used the photometric system coefficients defined in SDSS for the used field. The accuracy of zero-point determination was ~ 0.01 mag in all filters.

3 RESULTS

3.1 Spectra and oxygen abundance

The spectra of regions **a** and **b**, obtained on 2009.01.22, are shown in the top and bottom panels of Fig. 2, respectively.

³ The Nançay Radioastronomy Station is part of the Observatoire de Paris and is operated by the Ministère de l’Education Nationale and Institut des Sciences de l’Univers of the Centre National de la Recherche Scientifique.

⁴ <http://www.astro.princeton.edu/PBOOK/science/galaxies/galaxies.htm>

Table 2. Line intensities in ‘composite’ spectra of H II regions **a** and **b**

$\lambda_0(\text{\AA})$ Ion	2008.11.26		2009.01.21		2009.01.22		2009.02.19	
	$F/F(\text{H}\beta)$	$I/I(\text{H}\beta)$	$F/F(\text{H}\beta)$	$I/I(\text{H}\beta)$	$F/F(\text{H}\beta)$	$I/I(\text{H}\beta)$	$F/F(\text{H}\beta)$	$I/I(\text{H}\beta)$
3727 [O II]	55.5±8.9	52.8±8.9	24.5±29.4	24.5±29.4	43.3±9.8	43.6±10.9	58.5±7.8	55.9±8.4
4101 H δ	20.1±2.8	26.4±4.5	25.1±3.4	25.1±3.4	9.7±1.3	24.4±4.4	12.0±1.5	28.4±5.0
4340 H γ	39.3±3.8	42.9±4.7	48.3±3.8	48.3±3.8	38.1±2.2	48.4±3.4	34.7±1.6	46.8±2.9
4363 [O III]	6.4±2.9	6.1±2.9	6.0±2.7	6.0±2.7	4.6±1.7	4.3±1.8	5.2±1.2	4.7±1.3
4861 H β	100±5.5	100±6.0	100±5.1	100±5.9	100±3.8	100±3.9	100±3.5	100±4.0
4959 [O III]	57.4±4.0	55.0±4.0	61.1±4.0	61.1±4.0	64.0±3.0	57.7±3.1	57.9±2.4	51.3±2.4
5007 [O III]	171±8.2	163±8.2	182±7.9	182±7.9	188±6.3	168±6.3	182±5.7	160±5.6
5876 He I	10.7±1.8	10.2±1.8	9.2±2.4	9.2±2.4	9.0±1.7	7.6±1.6	8.5±0.8	7.2±0.8
6548 [N II]	1.7±2.0	1.7±2.0	0.3±1.5	0.2±1.3	1.0±0.8	0.9±0.7
6563 H α	283±12.6	272±13.8	335±10.4	277±10.3	327±9.0	275±9.3
6584 [N II]	5.9±3.7	5.6±3.7	0.8±3.2	0.7±2.9	3.4±1.9	2.8±1.8
C(H β) dex	0.00±0.06		0.00±0.07		0.14±0.04		0.10±0.04	
EW(abs) \AA	2.75±0.72		0.00±2.38		5.25±0.45		5.90±0.43	
$F(\text{H}\beta)^a$	5.12±0.20		6.33±0.23		7.31±0.19		5.14±0.15	
EW(H β) \AA	55.2±2.1		81.2±3.0		52.0±1.4		48.0±1.2	
V_{hel} km s $^{-1}$	567±66		558±12		465±30		492±39	

^a in units of 10^{-16} ergs s $^{-1}$ cm $^{-2}$.

Table 3. Abundances derived from ‘composite’ spectra of regions **a** and **b**

Value	2008.11.26	2009.01.21	2009.01.22	2009.02.19
$T_e(\text{OIII})(10^3 \text{ K})$	21.46±6.72	19.72±5.32	17.12±3.73	18.66±2.84
$T_e(\text{OII})(10^3 \text{ K})$	16.08±1.62	15.58±5.34	14.71±3.84	15.42±2.90
$N_e(\text{SII})(\text{cm}^{-3})$	10±10	10±10	10±10	10±10
$\text{O}^+/\text{H}^+(\times 10^{-5})$	0.389±0.132	0.198±0.312	0.420±0.360	0.465±0.274
$\text{O}^{++}/\text{H}^+(\times 10^{-5})$	0.808±0.498	1.075±0.602	1.360±0.679	1.049±0.345
$\text{O}/\text{H}(\times 10^{-5})$	1.197±0.515	1.273±0.678	1.780±0.768	1.515±0.441
$12+\log(\text{O}/\text{H})$	7.08±0.19	7.10±0.23	7.25±0.19	7.18±0.13

The fluxes of these two regions are low, with a S-to-N ratio in the principal line [O III] $\lambda 4363$ of ~ 2 – 3 only. Due to the strong noise in the ultra-violet, the important line [O II] $\lambda 3727$ has also a low S-to-N ratio. The situation is similar for spectra obtained during the other nights.

The main goal of our spectral observations was to get the most reliable estimate of the galaxy parameter O/H from the data on the H II regions **a** and **b**. Due to the low quality of individual measurements, it is necessary to average all of them together. However, the seeing during two of four nights was somewhat poor ($1''.9$ - $2''.3$) to resolve these regions as individual in our 2D spectra. To use all spectral data in the most efficient way, we employ the following approach.

First, we have checked how robust is the estimate of O/H for two adjacent H II regions with the same O/H, but somewhat different physical conditions and emission line relative intensities, if we measure them first separately and second, as one entity. We have simulated the artificial ‘sum’ spectrum of this one entity, just summing up fluxes of all lines in the two individual spectra. The latter were chosen to have the line intensity ratios similar to the observed ones. As one could expect from the general principle of analytic functions, the resulting physical parameters appeared halfway between those for individual objects, and the O/H, in turn, to be very close (within 0.01 dex) to the single value

of the two individual objects. Since the sum spectra of regions **a** and **b** also have better S-to-N ratio than the spectra of individual components, assuming that their O/H are the same, we decided to extract in all four independent 2D spectra the same region of 21 rows (or $7.5''$) along the slit, which includes both regions and gives us 1D spectra with the sum of fluxes of both regions.

In Table 2, we present the line intensities $F(\lambda)$ of all relevant emission lines measured in all four obtained ‘composite’ spectra, integrated over the region with extent of 21 pixel along the slit, which includes both regions **a** and **b**, normalised by the intensity of H β , and $I(\lambda)$, corrected for the foreground extinction $C(\text{H}\beta)$ and the equivalent widths of underlying Balmer absorption lines $\text{EW}(\text{abs})$.

In Table 3 we present the electron temperatures for zones of emission of [O III] and [O II], the accepted electron densities N_e , and the ionic abundances of oxygen, along with the total abundances derived for the above measured line intensities with the classic T_e method, according to the scheme described in Kniazev et al. (2008).

To emphasise the consistency of the results of all nights, we summarise the values of O/H for these four ‘composite’ spectra with some relevant spectral parameters in the top part of Table 4. The values of O/H are the same within their quite large uncertainties, with the range of $12+\log(\text{O}/\text{H})$ of

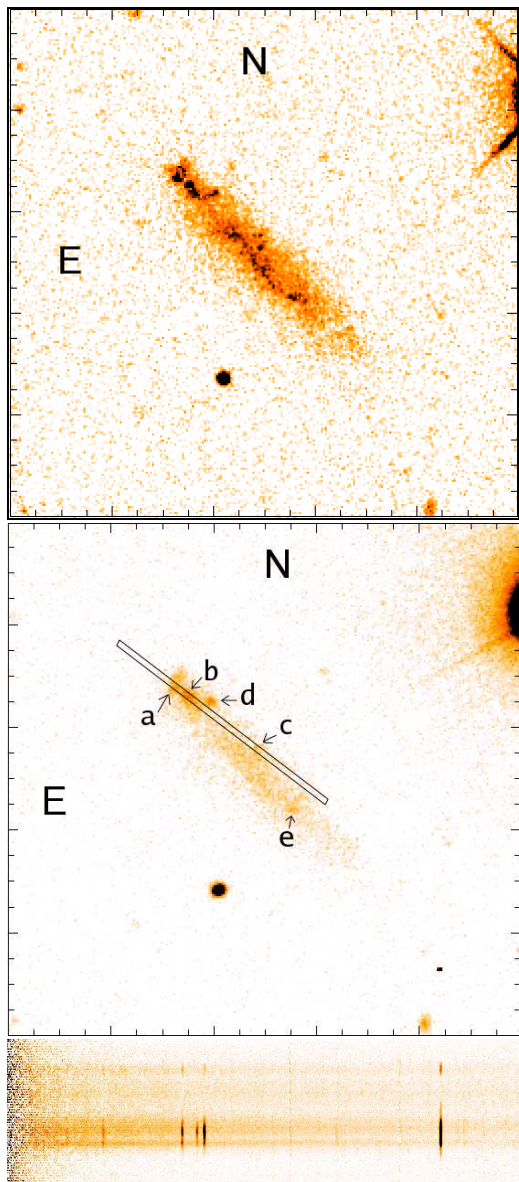


Figure 1. **Top panel:** The g -filter image of SDSS J0926+3343 obtained from the SDSS database. The total size of the field is $100''$ by $100''$. Some ‘knots’ at the NE edge are faint H II regions. The brightness enhancement seen as a ridge near the LSBD centre along the major axis looks like quite curved and patchy, indicating relatively recent SF episode. **Middle panel:** Two faint H II regions **a**, **b** ($\sim 4''$ in between) at the NE edge of galaxy disc and region **c** closer to the galaxy centre (indicated by arrows) are shown in the BTA H α -filter (SED665) image with the position of the long slit overlaid (PA= 54°). The regions **d**, mentioned in Sect. 3.3, and the faint H II-region **e**, for which the SDSS spectrum was obtained, are also indicated. The size of the field is $100''$ by $100''$. In the **bottom panel** the BTA 2D spectrum of SDSS J0926+3343 is shown with the emission of H II regions **a**, **b** in the lower part, and the faint emission of the H II region **c** seen in the upper part of spectrum.

7.08 ± 0.19 to 7.25 ± 0.19 . We accept their weighted mean as the best estimate of the galaxy O/H general mean, which corresponds to $12 + \log(\text{O}/\text{H}) = 7.16 \pm 0.05$.

The S-to-N ratio in the principal faint line [O III] $\lambda 4363$ is quite low in all analysed spectra; this leads to large errors in T_e and, respectively, to large errors in the derived O/H values. In such cases, or when [O III] $\lambda 4363$ is not detected, in the low-metallicity regime, Izotov & Thuan (2007) proposed the so-called semi-empirical method which employs the relation between the total relative intensity of lines [O III] $\lambda\lambda 4959, 5007$ and [O II] $\lambda 3727$ and T_e (see the similar method for the high-metallicity regime in Pagel et al. 1979; Shaver et al. 1983). This method was tested on several of the most metal-poor H II-regions in Izotov & Thuan (2007) and also by us on our own data. The O/H values, derived by this method, appeared to be well consistent, within rather small errors, with those derived via the direct T_e -method. The calculations of O/H are performed on the same formulae as described above in the direct method, but instead of T_e derived through the intensity ratio of [O III] lines $\lambda 4363$ and $\lambda\lambda 4959, 5007$, we accept T_e derived with the empirical formula from Izotov & Thuan (2007). The resulting values of O/H for each of the nights are shown in the bottom of Table 4. The respective values of $12 + \log(\text{O}/\text{H})$ vary in a significantly narrower range of 7.08 ± 0.10 to 7.12 ± 0.05 . Their weighted mean corresponds to $12 + \log(\text{O}/\text{H}) = 7.11 \pm 0.01$. The latter estimate is partly independent on that derived with the direct T_e -method since it does not use the intensity of [O III] $\lambda 4363$ line. Therefore, both the estimates of the galaxy O/H can be further averaged (with weights), that results in the ‘final’ value of O/H in SDSS J0926+3343 of $12 + \log(\text{O}/\text{H}) = 7.12 \pm 0.02$.

3.2 H I parameters

The profile of the 21-cm H I line emission in SDSS J0926+3343 obtained with the NRT is shown in Fig. 3. Its parameters are as follows. The integrated H I flux $F(\text{H I}) = 2.54 \pm 0.07$ Jy km s $^{-1}$. The central velocity of the profile is 536 ± 2 km s $^{-1}$. The profile widths are $W_{50} = 47.4 \pm 3$ km s $^{-1}$ and $W_{20} = 80.5 \pm 7$ km s $^{-1}$.

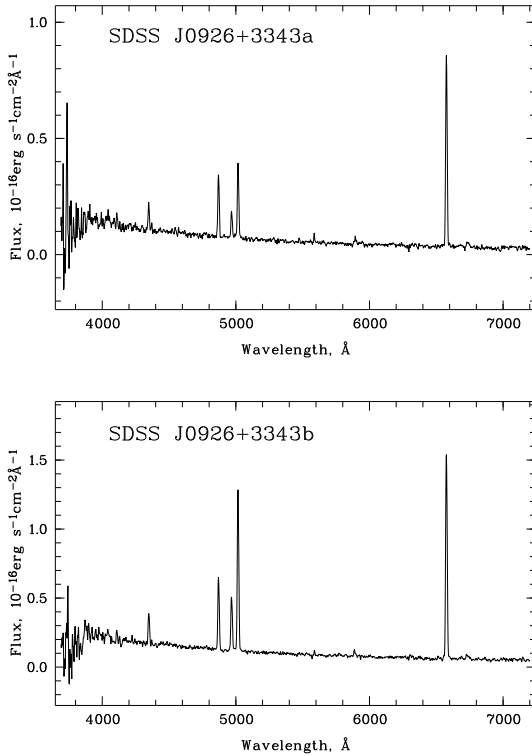
To estimate the galaxy global parameters, we accepted for its distance the value $D = 10.7$ Mpc (with the respective scale of 52 pc in $1''$). The latter comes from its $V_{\text{LG}} = 488$ km s $^{-1}$, the accepted Hubble constant of 73 km s $^{-1}$ Mpc $^{-1}$ and the correction for the large negative peculiar velocity, discussed by Tully et al. (2008), which we adopt for this region as 290 km s $^{-1}$. The H I mass of the galaxy is determined by the well-known relation for optically thin H I-line emission from Roberts (1969) that gives $M(\text{H I}) = 6.8 \times 10^7 M_\odot$.

3.3 Photometric properties and the age estimates

From the surface brightness radial profiles in g and r filters shown in Fig. 4, one can derive the colour of the underlying ‘exponential disc’ $(g - r) = \sim 0.10$. Using transformation formula of Lupton et al. (2005), this translates to the relation $\mu_B = \mu_g + 0.25$ mag arcsec $^{-2}$. Then, from the galaxy SB profile in g -filter, the ‘optical’ radius R_{opt} at $\mu_B = 25$ mag arcsec $^{-2}$ and the Holmberg radius R_{H0} at

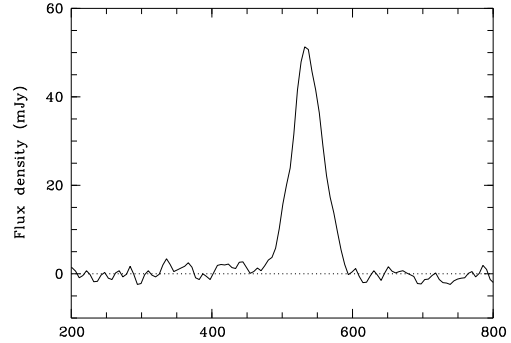
Table 4. Spectral parameters and O/H for the four SDSS J0926+3343 ‘composite’ spectra

Run/Date	2008.11.26	2009.01.21	2009.01.22	2009.02.19
O/H derived via direct T_e method				
C(H β)	0.00 \pm 0.06	0.00 \pm 0.07	0.14 \pm 0.04	0.10 \pm 0.04
EW(abs)	2.8 \pm 0.7	0.0 \pm 2.4	5.4 \pm 0.4	5.9 \pm 0.4
I(4363)/I(H β)	0.064 \pm 0.029	0.060 \pm 0.027	0.046 \pm 0.017	0.052 \pm 0.017
I(4959+5007)/I(H β)	2.28 \pm 0.09	2.44 \pm 0.09	2.52 \pm 0.07	2.40 \pm 0.06
I(3727)/I(H β)	0.55 \pm 0.09	0.24 \pm 0.29	0.43 \pm 0.10	0.59 \pm 0.08
O/H (in 10^{-5})	1.197 \pm 0.515	1.273 \pm 0.678	1.780 \pm 0.769	1.515 \pm 0.441
12+log(O/H)	7.08 \pm 0.19	7.10 \pm 0.23	7.25 \pm 0.19	7.18 \pm 0.13
O/H derived via semi-empirical method of Izotov & Thuan				
O/H (in 10^{-5})	1.331 \pm 0.156	1.199 \pm 0.278	1.285 \pm 0.157	1.322 \pm 0.149
12+log(O/H)	7.12 \pm 0.05	7.08 \pm 0.10	7.11 \pm 0.05	7.12 \pm 0.05

**Figure 2.** Spectra with resolution of 12 Å of regions **a** (top panel) and **b** (bottom panel) in SDSS J0926+3343, obtained on 2009 January 22.

$\mu_B=26.5$ mag arcsec $^{-2}$ are $R_{\text{opt,eff}}=9''.4$ and $R_{\text{Ho,eff}}=19''.7$. To transform these effective radii to real ones, the correction factor $(b/a)^{-1/2}=1.89$ should be applied, where the galaxy axial ratio $b/a=0.28$ was adopted from NED/SDSS. This results in the ‘optical’ radius of $R_{\text{opt}}=17''.8$ (~ 0.93 kpc) and in the ‘Holmberg’ radius of $R_{\text{Ho}}=37''.2$ (~ 1.94 kpc).

From the above exponential disc fits (for internal regions with $R < 12''$) we also estimated the central SB and disc scale lengths. The best fits are for g and r filters, which give $\mu_g^0=23.32$ and $\mu_r^0=23.28$ mag arcsec $^{-2}$ with respective scale lengths of $6''.6$ and $7''.2$. Their mean $6''.9$ corresponds

**Figure 3.** The NRT profile of H I-line emission from SDSS J0926+3343. X-axis shows radial heliocentric velocity in km s $^{-1}$. Y-axis shows the galaxy flux density in mJy.

to the linear scale length of 0.36 kpc. When corrected for $(b/a)^{-1/2}$, this gives a radial disc scale length of 0.68 kpc. With the same magnitude transform as above, we derive the *observed* central blue SB $\mu_B^0=23.48$ mag arcsec $^{-2}$ (after correction for $A_B=0.08$). Due to almost edge-on orientation of the galaxy disc, its observed central SB is significantly enhanced. We correct the latter value, taking the visible axial ratio $p = b/a=0.28$ and adopting the internal axial ratio $q=0.20$. The inclination angle i , derived from the well known formula: $\cos(i)^2 = (p^2 - q^2)/(1 - q^2)$, amounts to $i = 78.5^\circ$. The respective correction for μ_B^0 is equal to 1.75 mag arcsec $^{-2}$. Thus, the central SB corrected for inclination appears very low: $\mu_B^0=25.39$ mag arcsec $^{-2}$, and this galaxy should be classified as a ‘Very Low Surface Brightness’.

The measured u, g, r, i magnitudes and the derived, Galaxy extinction corrected colours $(u-g)$, $(g-r)$ and $(r-i)$ are presented in Table 5. In the first line we give the parameters for the whole galaxy. In the second line – for the whole galaxy with removal of the light of H II regions **a**, **b**, **c** and the small blue nebosity **d** somewhat outside the main disc, at $\sim 5''$ west of region **b**. The parameters in the two last lines are discussed below.

Our main goal is to compare the observed colours of stellar population with the PEGASE2 model evolutionary tracks (Fioc & Rocca-Volmerang 1999), in order to obtain

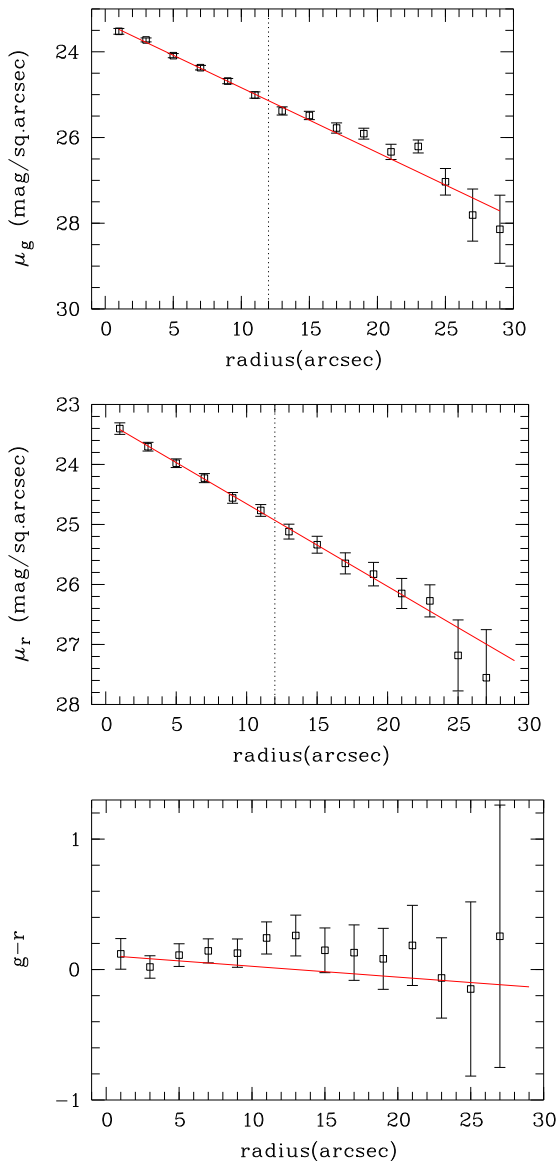


Figure 4. SDSS J0926+3343 surface brightness in g and r filters and $g - r$ colour versus the effective radius. The solid lines show model fits for exponential discs on the profile part with $<12''$ (shown by vertical dotted line).

the estimates of the maximal stellar ages in the galaxy. As one can see from the $(g - r)$ colour radial profile in Fig. 4, due to the contribution of the mentioned H II regions to the light of the outer parts of the galaxy, it is difficult to estimate from the profile the outer colours and decide whether there is a colour gradient in the underlying stellar population. Also, due to the very elongated form of the galaxy, the photometry in ring diaphragms mixes the light from different parts of the ‘disc’, and thus will tend to wash-up colour gradients if they are present. Therefore, to analyse the stellar light colours of the galaxy outer parts, we employ the approach, used in our analysis of the stellar colours in the galaxy DDO 68 (Pustilnik et al. 2008a).

First, to address the possible colour differences, we measured the light of the central ‘ridge’, the elongated struc-

ture along the ‘disc’ major axis with somewhat enhanced SB. This was done by summing up the light of ten round diaphragms with 3 pixels radius ($\sim 1''.2$) placed along the ‘ridge’. Its parameters are given in the third line of Table 5. As one can see, the ‘ridge’ colours are very close to those of the total ‘disc’, with the $(g - r)$ colour probably to be a bit bluer. To estimate the colours of the ‘outer’ region, we performed the similar photometry in the regions, adjacent to the ‘ridge’, summing-up the light from twelve diaphragms of the same size, in which the signal in all filters was above the background noise level. This area was limited by the extent in u -filter. The derived parameters of this ‘outer’ region are shown in the fourth line of Table 5. Its $(u - g)$ colour appears marginally redder, while the $(g - r)$ and $(r - i)$ are consistent within their errors with the colours of the ‘ridge’ and the whole galaxy.

In Fig. 5 we compare the derived colours in Table 5 with the model tracks from the PEGASE2 package. We used the standard Salpeter IMF and the metallicity $Z=0.0004$, which is the best proxy to the value found from our spectroscopy of H II regions. We show the evolutionary tracks for the two extreme SF laws to derive the upper limit of the visible stellar population ages. The integrated colours of the disc ‘sit’ in between of continuous and instantaneous SF law tracks. Its rather blue colour $(g - r)$ corresponds to ages from ~ 0.7 to ~ 2.5 Gyr, depending on the SF law. The ugr colours of the ‘ridge’ are better consistent with instantaneous starburst occurred several hundred Myr ago. The ugr colours of the ‘outer’ region appear a bit offset from the continuous SF track, but accounting for the observed colour errors, the difference is not significant. The nearest part of the track (in terms of amount of σ_{err} and the related probability) corresponds to the ages of stellar population of ~ 1 –3 Gyr. That is, within the limits of measurable LSB periphery, the oldest visible stellar population appears quite young (~ 2 Gyr), in difference with the absolute majority of thousands galaxies, for which the similar data are acquired. In the gri colour plot (not shown) both tracks go too close each to other, so the galaxy gri colours alone would be inconclusive. However, the measured $(r - i)$ colours are consistent with the above conclusions derived from ugr colours.

4 DISCUSSION

In Table 6 we present the main parameters of the studied galaxy. From the total magnitudes in filters g and r (Table 5), with the transformation equations of Lupton et al. (2005), we derive the total B -band magnitude, $B_{\text{tot}}=17.34\pm 0.03$. For the accepted distance modulus of SDSS J0926+3343 $\mu=30.16$ ($D=10.7$ Mpc and $A_B=0.08$) its absolute magnitude $M_B^0 = -12.90$. The latter corresponds to $L_B=2.24\times 10^7 L_{B\odot}$. Then, from the $M(\text{HI})$ derived in the previous section, one obtains the ratio $M(\text{HI})/L_B \sim 3.0$ (in solar units). This value is rather large for the Local Universe galaxies and is among the few per cent highest ratios ever measured.

From the HI line width at 20%-level of the maximum intensity, W_{20} , one can estimate the maximal rotational velocity, using the standard approximation, as, e.g., formula (12) from Tully & Fouqué (1985). Since the galaxy is seen almost edge-on, the inclination correction is

Table 5. Magnitudes and colours of SDSS J0926+3343 and its regions

Region	$u \pm err_u$	$g \pm err_g$	$r \pm err_r$	$i \pm err_i$	$(u-g)^0 \pm err$	$(g-r)^0 \pm err$	$(r-i)^0 \pm err$
Total light	17.95 0.08	17.08 0.03	16.98 0.04	16.96 0.04	+0.87 0.08	+0.08 0.05	-0.06 0.06
Total with removed H II	18.04 0.08	17.14 0.03	17.03 0.04	17.01 0.04	+0.88 0.08	+0.09 0.05	+0.01 0.06
The ‘ridge’	20.44 0.11	19.54 0.04	19.53 0.06	19.55 0.08	+0.88 0.11	-0.01 0.07	-0.03 0.10
The outer region	20.55 0.14	20.00 0.06	19.90 0.10	19.90 0.13	+0.52 0.15	+0.08 0.12	-0.02 0.16

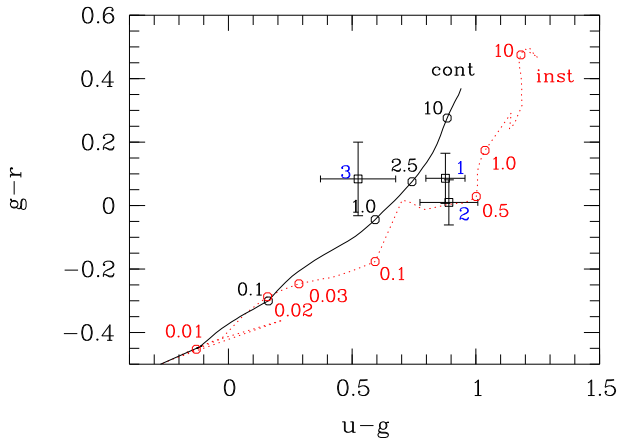


Figure 5. The $(u-g)$, $(g-r)$ colours of SDSS J0926+3343, corrected for the small extinction in the Galaxy, compared with the PEGASE2 evolutionary tracks for the standard Salpeter IMF and $Z=0.0004$. The two extremes of the SF law are shown: continuous with constant SF (solid line) and instantaneous SF (dashed line). Open circles along the tracks mark the time in Gyr elapsed since the beginning of SF. The point labelled “1” indicates the integrated colours of the galaxy, excluding the four mentioned small H II-regions. The point labelled “2” represents the colours of the ‘ridge’ (Fig. 1, top panel). The point labelled “3” represents the colours of the outer part adjacent to the ‘ridge’ region (see description in text). If interpreted in terms of the colours, nearest to a model evolutionary track, the latter best correspond to the continuous SF for ages of $T \sim 1-3$ Gyr.

only 1.02. For a measured line width $W_{20} = 80.5 \text{ km s}^{-1}$, the derived $V_{\text{rot}} \sim 31.2 \text{ km s}^{-1}$, and the inclination corrected $V_{\text{rot}} \sim 32 \text{ km s}^{-1}$, which is typical of dwarf galaxies with comparable M_B in the faint dwarf sample FIGGS of Begum et al. (2008b). Having V_{rot} and the characteristic size of the galaxy, one can estimate its total (dynamical) mass which is necessary to balance the centrifugal force within a certain radius.

The typical radii of HI discs (at the column density level of $10^{19} \text{ atoms cm}^{-2}$) in dwarf galaxies with $M_B \sim -13$, close to that of this LSB dwarf, are 2.5-3 times larger than the Holmberg radius (e.g., Begum et al. 2008a,b). Therefore, we accept that the HI radius of this galaxy is $2.7 R_{\text{H0}}$, that is $R_{\text{HI}} = 5.2 \text{ kpc}$. Then, from the relation $M(R < R_{\text{HI}}) = V_{\text{rot}}^2 \times R_{\text{HI}}/G$, where G is the gravitational constant, one derives the total mass within R_{HI} as follows: $M_{\text{tot}} = 12.4 \times 10^8 M_{\odot}$. To get the estimate of the galaxy gas mass, we sum $M(\text{HI})$ and $M(\text{He})$ (a fraction of 0.33 of HI mass) that gives $M_{\text{gas}} = 9.04 \times 10^7 M_{\odot}$.

The mass of stars can be estimated as follows. We take

from Table 5 the total g -magnitude of the LSB disc (without light of H II regions), equal to 17.14. We also account for the light contribution of the younger stellar population of the ‘ridge’, of the order of 10 % in g -filter. Then, the improved estimate of the LSB disc g -filter magnitude is 17.24. This corresponds to the extinction-corrected absolute magnitude $M_g = -13.0$. According to the PEGASE2 model track with continuous SF and constant SF rate, for $T=2.5$ Gyr, the colour $g-V = -0.08$, that is its $M_V^0 = -12.92$. Accounting that for this PEGASE2 track, the luminosity of a star cluster with $T=2.5$ Gyr corresponds to the luminosity of $V=6.47$ mag per $1 M_{\odot}$, which is fainter than the galaxy estimated M_V^0 by 19.39 mag, we obtain that the full stellar mass (with $T=2.5$ Gyr) of the galaxy is $M_{\text{star}} \sim 5.70 \times 10^7 M_{\odot}$. This implies that the total baryonic mass $M_{\text{bary}} = 1.47 \times 10^8 M_{\odot}$ and the gas mass-fraction $\mu_g = M_{\text{gas}}/(M_{\text{gas}} + M_{\text{star}}) = 0.61$. With the mass ratio $M_{\text{tot}}/M_{\text{bary}} = 8.3$, this LSBD galaxy is clearly a Dark-Matter dominated one. To get a better precision estimate of the DM halo mass and its radial distribution, one needs HI mapping of the galaxy.

Having all these unusual properties in one object (the record-low value of O/H, ‘young’ ($T \sim 2 \pm 1$ Gyr) main stellar population, large gas-mass fraction), the galaxy SDSS J0926+3343 represents a nice nearby laboratory to study several cosmologically related issues. This looks to be very isolated dwarf galaxy (the nearest luminous galaxies are at $D > 2$ Mpc) and, thus, provides a good opportunity to study the SF, induced presumably by the internal instabilities in the most metal-poor environment and at quite low disc baryonic surface densities. The star ‘clusters’ or ‘stellar associations’ responsible for ionisation of H II regions **a** and **b**, according to the values of their $\text{EW}(\text{H}\beta)$ are quite young, having ages of 7–8 Myr. Therefore, one can hope to find in them individual massive stars with $Z \sim Z_{\odot}/35$, similar to, e.g., the LBV star in that low- Z dwarf galaxy DDO 68 (Pustilnik et al. 2008b; Izotov & Thuan 2009).

Studying gas kinematics in this LSBD may determine the density distribution of the DM halo, and thus, better constrain the DM nature. There is still a chance that this LSBD galaxy experiences a substantial external disturbance, since its disc looks somewhat warped, and its main SF sites are situated at large distances from the galaxy centre. However, the alternative option of triaxial DM halo can also explain the visible warps in this LSBD disc (e.g., Jeon, Kim & Ann 2009). In particular, HI maps with the angular resolution of $5'' - 10''$ would help to elucidate the neutral gas morphology and kinematics and to check the hypothesis of an intergalactic HI cloud infall or a minor merger.

Looking at this unusual galaxy in a more general aspect, one can notice its appearance in the nearby Lynx-Cancer void, where other very metal-poor and unevolved

dwarf galaxies are found. They include, in particular, DDO 68 at the mutual distance to SDSS J0926+3343 of only ~ 1.6 Mpc (Pustilnik et al. 2005), and HS 0822+3542 and SAO 0822+3542 (Pustilnik et al. 2003). A few XMD dwarf galaxies in the region of this void found by Izotov & Thuan (2007), as well as several more such galaxies found by us, will be presented in a forthcoming paper.

In Table 6, along with the data for SDSS J0926+3343, we present the properties of DDO 68, in order to emphasise the range of parameters in two ‘neighbouring’ most metal-poor dwarf galaxies residing in the Lynx-Cancer void. The blue luminosity and the gas mass of DDO 68 are higher by an order of magnitude, while its optical size is larger by a factor of ~ 5 . The DDO 68 morphology, kinematics and stellar colours imply that its appearance is related to the recent merger (~ 1 Gyr ago) of two very gas-rich and very metal-poor dwarf galaxies (or gas clouds/protogalaxies).

The increased density of such rare objects in this region is certainly not by chance. XMD galaxies seem to prefer residence in some selected regions. Our findings indicate that while the fraction of such galaxies is small, namely the void environment is favourable for the retarded dwarf galaxy formation and their slower evolution. The well-known interacting/merging pair of the most metal-poor dwarf galaxies SBS 0335–052E,W (see new data in Ekta, Pustilnik & Chengalur 2009; Izotov et al. 2009) is also situated near the border of a large void (Peebles 2001). The existence of the sizable HI cloud population in ‘nearby’ voids, with the baryonic masses comparable to those of dwarf galaxies, visible through their Ly- α absorption (Manning 2002, 2003, and references therein), also hints on the unevolved state of the significant fraction of baryons in voids. The more advanced analysis of the Lynx-Cancer void dwarf galaxy census and the summary of their properties will be presented elsewhere.

Summarising the results and discussion above, we draw the following conclusions:

(i) The edge-on VLSB ($\mu_B^0=25.4$ mag arcsec $^{-2}$) dwarf galaxy SDSS J0926+3343 is situated in the nearby Lynx-Cancer void. It has several faint HII regions. For the two brightest of them, **a** and **b**, at the NE edge, we obtained optical spectra and derived their oxygen abundance. The general means of their O/H values derived by the direct T_e and by the semi-empirical method of Izotov & Thuan (2007) are well consistent with each other, yielding $12+\log(\text{O}/\text{H})$ of 7.16 ± 0.05 and 7.11 ± 0.01 , respectively. We accepted the mean of the two, $12+\log(\text{O}/\text{H})=7.12\pm 0.02$, as the measure of O/H in the galaxy.

(ii) SDSS J0926+3343 appeared the most metal-poor galaxy in the Local Universe, situated in the remarkable proximity (~ 1.6 Mpc) to another that low metallicity dwarf galaxy DDO 68 (with $12+\log(\text{O}/\text{H})=7.14$).

(iii) The HI integrated flux and the velocity width data for this galaxy, along with the optical photometry and the size estimates, indicate the very gas-rich object, with $M(\text{HI})/L_B \sim 3.0$ and with the derived gas mass-fraction of $\mu_g \sim 0.6$. The galaxy is a DM dominated, with the estimated mass ratio of $M_{\text{tot}}/M_{\text{bary}} \sim 8.3$.

(iv) The $(u-g)$, $(g-r)$ and $(r-i)$ colours of SDSS J0926+3343 are ‘blue’. The ‘outer’ region colours well match the PEGASE2 model track for the evolving stellar popula-

Table 6. Main parameters of SDSS J0926+3343 and DDO 68

Parameter	J0926+3343	DDO 68
R.A.(J2000.0)	09 26 09.45	09 56 45.7
DEC.(J2000.0)	+33 43 04.1	+28 49 35
A_B (from NED)	0.08	0.08
B_{tot}	$17.34\pm 0.03^{(2)}$	14.74
$V_{\text{hel}}(\text{HI})(\text{km s}^{-1})$	$536\pm 2^{(3)}$	$502\pm 2^{(9)}$
$V_{\text{LG}}(\text{HI})(\text{km s}^{-1})$	$488\pm 2^{(3)}$	428
Distance (Mpc)	$10.7^{(2)}$	$9.9^{(2)}$
M_B^0 (4)	-12.90	-15.32 $^{(2)}$
Opt. size ($''$) ⁵	$35.8\times 9.9^{(2)}$	$103\times 38^{(8)}$
Opt. size (kpc)	$0.93\times 0.26^{(2)}$	4.94×1.82
μ_B^0 (mag arcsec $^{-2}$)	$25.4^{(2)}$	$< 22.7^{(8)}$
$12+\log(\text{O}/\text{H})$	$7.12\pm 0.02^{(2)}$	$7.14\pm 0.03^{(10)}$
HI int.flux ⁽⁶⁾	$2.54\pm 0.07^{(2,3)}$	28.9 ± 3.0
W_{50} (km s $^{-1}$)	$47.4\pm 3^{(2,3)}$	$82^{(9)}$
W_{20} (km s $^{-1}$)	$80.5\pm 7^{(2,3)}$	$105^{(9)}$
$V_{\text{rot}}(\text{HI})(\text{km s}^{-1})$	$32^{(2,3)}$	$52^{(9)}$
$M(\text{HI})$ ($10^7 M_\odot$)	$6.8^{(2)}$	$66.8^{(2)}$
M_{dyn} ($10^7 M_\odot$)	$124^{(2)}$	487
$M(\text{HI})/L_B$ ⁽⁷⁾	$3.0^{(2)}$	$2.9^{(9)}$
T(main star population)	$1-3$ Gyr $^{(2)}$	$\lesssim 1$ Gyr $^{(11)}$

(1) – from NED; (2) – derived in this paper; (3) – derived from NRT HI profile; (4) – corrected for Galactic extinction $A_B=0.08$; (5) – $a \times b$ at $\mu_B = 25.4$ mag arcsec $^{-2}$; (6) – in units of $\text{Jy}\cdot\text{km s}^{-1}$; (7) – in solar units; (8) Pustilnik et al. (2005); (9) - Ekta et al. (2008); (10) - Izotov & Thuan (2007); (11) - Pustilnik et al. (2008a).

tion with continuous SF for ages of $T\sim 1-3$ Gyr. Thus, all three observational parameters: O/H, μ_g and blue colours are consistent with an evolutionary young status of this LSB dwarf galaxy.

ACKNOWLEDGEMENTS

SAP and ALT acknowledge the support of this work through the RFBR grant No. 06-02-16617. SAP is also grateful for the support through the Russian Federal Agency of Education grant No. 2.1.1/1937. SAP, ALT and AYK acknowledge the BTA TAC for the continuous support of this project at the SAO 6-m telescope. The authors thank A. Valeev for the help with BTA observation. SAP and JMM acknowledge the NRT TAC for allocation of time for this program in 2007. The authors thank the reviewer D. Saikia for useful suggestions which improved the paper presentation. The authors acknowledge the spectral and photometric data and the related information available in the SDSS database used for this study. The Sloan Digital Sky Survey (SDSS) is a joint project of the University of Chicago, Fermilab, the Institute for Advanced Study, the Japan Participation Group, the Johns Hopkins University, the Max-Planck-Institute for Astronomy (MPIA), the Max-Planck-Institute for Astrophysics (MPA), New Mexico State University, Princeton University, the United States Naval Observatory, and the University of Washington. Apache Point Observatory, site of the SDSS telescopes, is operated by the Astrophysical Research Consortium (ARC). This research has made use of the NASA/IPAC Extragalactic Database (NED), which is oper-

ated by the Jet Propulsion Laboratory, California Institute of Technology, under contract with the National Aeronautics and Space Administration.

REFERENCES

- Abazajian K.N., Adelman-McCarthy J.K., Agüeros M.A. et al., 2009, *ApJS*, 182, 543
- Afanasiev V.L., Moiseev A.V., 2005, *Astron. Lett.*, 31, 193
- Arkhipova N.A., Komberg B.V., Lukash V.N., Mikheeva E.V., 2007, *Astr.Rep.* 51, 787
- Begum A., Chengalur J.N., Karachentsev I.D., Sharina M.E., 2008a, *MNRAS*, 386, 138
- Begum A., Chengalur J.N., Karachentsev I.D., Sharina M.E., Kaisin S.S., 2008b, *MNRAS*, 386, 1667
- Bohlin R.C., 1996, *AJ*, 111, 1743
- Chengalur J.N., Pustilnik S.A., Martin J.-M., Kniazev A.Y., 2006, *MNRAS*, 371, 1849
- Cross N., Driver S.P., 2002, *MNRAS*, 329, 579
- Ekta, Chengalur J.N., Pustilnik S.A., 2008, *MNRAS*, 391, 881
- Ekta B., Pustilnik S.A., Chengalur J.N., 2009, *MNRAS*, 397, 963
- Fairall A., 1998, *Large-Scale Structures in the Universe*, Wiley-Praxis, 196 pp.
- Fioc M., Rocca-Volmerange B., 1999, *arXiv:astro-ph/9912179*
- Fukugita M., Ichikawa T., Gunn J.E., Doi M., Shimasaku K., Schneider D.P., 1996, *AJ*, 111, 1748
- Geha M., Blanton M.R., Masjedi M., West A.A., 2006, *ApJ*, 653, 240
- Gottlöber S., Lokas E.L., Klypin A., Hoffman Y., 2003, *MNRAS*, 344, 715
- Gunn J.E., Carr M.A., Rockosi C.M. et al., 1998, *AJ*, 116, 3040
- Hahn O., Carollo C.M., Porciani C., Dekel A., 2007, *MNRAS*, 381, 41
- Hahn O., Porciani C., Dekel A., Carollo C.M., 2009, *MNRAS*, accepted (*arXiv:0803.4211v2*)
- Haynes M., 2008, in J.I. Davies & M.J. Disney, eds, *Proc. of IAU Symposium 244, Dark Galaxies and Lost Baryons*, Cambridge Univ. Press, Cambridge, Vol. 244, p. 83
- Haynes M.P., Giovanelli R., Chincarini G.L., 1984, *ARA&A*, 22, 445
- Hoefl M., Yepes G., Gottlöber S., Springel V., 2006, *MNRAS*, 371, 401
- Izotov Y.I., Thuan T.X., Guseva N.G., 2005, *ApJ*, 632, 210
- Izotov Y.I., Thuan T.X., 2007, *ApJ*, 665, 1115
- Izotov Y.I., Thuan T.X., Guseva N.G., 2007, *ApJ*, 671, 1297
- Izotov Y.I., Thuan T.X., 2009, *ApJ*, 690, 1797
- Izotov Y.I., Guseva N.G., Fricke K.J., Papaderos P., 2009, *A&A*, accepted (*arXiv:0907.2116*)
- Jeon M., Kim S.S., Ann H.B., 2009, *ApJ*, 696, 1899
- Karachentsev I.D., Karachentseva V.E., Huchtmeier W.K., Makarov D.I., 2004, *AJ*, 127, 2031
- Kniazev A., Pustilnik S., Masegosa M. et al., 2000, *A&A*, 357, 101
- Kniazev A.Y., Pustilnik S.A., Grebel E.K., Lee H., Pramskij A.G., 2004a, *ApJS*, 153, 429
- Kniazev A.Y., Grebel E.K., Pustilnik S.A., Pramskij A.G., Kniazeva T.F., Prada F., Harbeck D., 2004b, *AJ*, 127, 704
- Kniazev A.Y., Zijlstra A., Grebel E.K. et al., 2008, *MNRAS*, 388, 1667
- Lupton R., Gunn J.E., Ivezić Z. et al., 2001, in: Harnden F.R., Jr., Primini F.A., & Payne H.E., eds, *Astronomical Data Analysis Software and Systems X*, ASP Conf. Ser. 238, Astron. Soc. Pac., San Francisco, p. 269
- Lupton R., et al. 2005, <http://www.sdss.org/dr5/algorithms/sdssUBVRIT>
- Manning C., 2002, *ApJ*, 574, 599
- Manning C., 2003, *ApJ*, 591, 79
- Martin J.-M., Gerard E., Colom P., Theureau G., Cognard I., 2002, in: Combes F. and Barret D., eds, *SF2A, EDP Sciences*, p. 237
- Mathis H., White S.D.M., 2002, *MNRAS*, 337, 1193
- Pagel B.E.J., Edmunds M.G., Blackwell D.E., Chun M.S., Smith G., 1979, *MNRAS*, 189, 95
- Patiri S.G., Prada F., Holtzman J., Klypin A., Betancort-Rijo J., 2006, *MNRAS*, 372, 1710
- Peebles P.J.E., 2001, *ApJ*, 557, 459
- Pier J.R., Munn J.A., Hindsley R.B., et al. 2003, *AJ*, 125, 1559
- Pustilnik S.A., Kniazev A.Y., Pramsky A.G., Ugryumov A.V., Masegosa J., 2003, *A&A*, 409, 917
- Pustilnik S.A., Kniazev A.Y., Pramskij A.G., 2005, *A&A*, 443, 91
- Pustilnik S.A., Martin J.-M., 2007, *A&A*, 464, 859
- Pustilnik S.A., Tepliakova A.L., Kniazev A.Y., 2008a, *Astron.Lett.*, 34, 457
- Pustilnik S.A., Tepliakova A.L., Kniazev A.Y., Burenkov A.N., 2008b, *MNRAS Lett.* 388, 24
- Roberts M.S., 1969, *AJ*, 74, 859
- Schneider S.E., Helou G., Salpeter E.E., Terzian Y., 1986, *AJ*, 92, 742
- Shaver P.A., McGee R.X., Newton L.M., Danks A.C., Potasz S.R., 1983, *MNRAS*, 204, 53
- Smith J.A., Tucker D.L., Kent S., et al. 2002, *AJ*, 123, 2121
- Sorrentino G., Antonuccio-Delogu V., Rifatto A., 2006, *A&A*, 460, 673
- Tully R.B., Fouqué P., 1985, *ApJ.Suppl.*, 58, 67
- Tully R.B., Shaya E.J., Karachentsev I.D., Courtois H.M., Kocevski D.D., Rizzi L., Peel A., 2008, *ApJ*, 676, 184
- York D.G., Adelman J., Anderson J.E. et al., 2000, *AJ*, 120, 1579
- Zackrisson E., Bergvall N., Östlin G., 2005, *A&A*, 435, 29

This paper has been typeset from a \TeX / \LaTeX file prepared by the author.